Facile synthesis of electrospun MFe_2O_4 (M = Co, Ni, Cu, Mn) spinel nanofibers with excellent electro-catalytic properties for oxygen evolution and hydrogen peroxide reduction

Mian Li,[a] Yueping Xiong,[b] Xiaotian Liu,[b] Xiangjie Bo,[a] Yufan Zhang,[a] Ce Han [a] and Liping Guo[*a]

[a] *Faculty of Chemistry, Northeast Normal University, Changchun, 130024, P. R. China*

[b] *School of Chemical Engineering and Technology, Harbin Institute of Technology, Harbin 150001, China*

[*] Corresponding author

Tel.: +86-0431-85099762.

Fax: +86-0431-85099762.

E-mail address: guolp078@nenu.edu.cn (L. Guo).

Experimental

Reagents and apparatus

Polyvinylpyrrolidone (PVP, K90), *N, N*-dimethylformamide (DMF), H_2O_2, glucose, uric acid (UA), dopamine (DA), ascorbic acid (AA), and acetaminophen (AP)

were obtained from Alfa Aesar. KOH, $Ni(NO_3)_2 \cdot 6H_2O$, $Cu(NO_3)_2 \cdot 3H_2O$, $Mn(CH_3COO)_2 \cdot 4H_2O$, $Co(NO_3)_2 \cdot 6H_2O$ (99.0 %), and $Fe(NO_3)_3 \cdot 9H_2O$ were purchased from Sinopharm Chemical Reagent C. All other reagents were of analytical grade and used as received. Highly purified nitrogen (≥ 99.99%) was supplied by Changchun Juyang Co Ltd. Ultrapure water (resistivity：$\rho \geq 18$ MΩ cm^{-1}) was used to prepare the solutions. Before the reduction and detection of H_2O_2, the 0.1 M KOH is bubbled with N_2 for 30 min to remove the dissolved oxygen.

All electrochemical experiments were performed on a CHI 830B electrochemical workstation (CH Instruments, China) connected to a personal computer in a traditional three-electrode configuration. A glassy carbon electrode (GCE, d = 3 mm), Ag/AgCl (in saturated KCl solution), and a platinum wire were served as working, reference, and counter electrodes, respectively. The current densities in this work were recorded as the ratios of currents to the geometric areas of the GCE (0.0707 cm^2).

The X-ray diffraction (XRD) patterns were obtained on an X-ray D/max-2200vpc instrument (Rigaku Corporation, Japan) operating at 40 kV and 20 mA, and using Cu K radiation (k = 0.1541 nm). The morphologies and compositions of these as-prepared samples were studied by Philips XL-30 ESEM equipped with an EDS analyzer. TEM images were obtained by using a JEM-2100F transmission electron microscope (JEOL, Japan) operating at 200 kV. The FT-IR spectra of samples were recorded by the Nicolet Magna 560 FT-IR spectrometer with a KBr plate. The nitrogen adsorption–desorption isotherms were performed on an ASAP 2020 (Micromeritics, USA). Before the measurements, samples were degassed in vacuum

at 150 °C for 6 h. The Brunauer–Emmett–Teller (BET) method was utilized to calculate the specific surface areas by using adsorption data. The pore size distribution was derived from the adsorption branches by using the Barrett–Joyner–Halenda (BJH) model. The total pore volume (V_t) was estimated from the adsorbed amounts at a relative pressure (P/P_0) of ca.1. X-ray photo-electron spectroscopy (XPS) was measured using Thermo ESCA LAB spectrometer (USA).

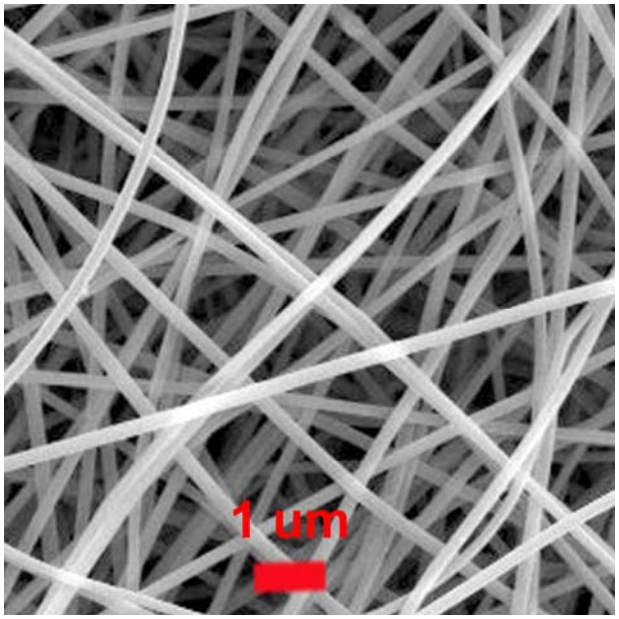

Fig. S1 SEM images of the as-collected $Co(NO_3)_2/Fe(NO_3)_3$/PVP precursor NFs.

Table S1 The C, O, M, and Fe components of MFe_2O_4 NFs (M = Co, Ni, Cu, and Mn) samples recorded from the EDS quantitative analyses.

Samples	C (at.%)	O (at.%)	Fe (at.%)	M (at.%)	Molar ratios of M: Fe: O
Fe_2O_3 NFs	6.45	53.42	42.02	–	–
$CoFe_2O_4$ NFs	4.57	57.51	25.26	12.66	1:1.995: 4.543
$NiFe_2O_4$ NFs	6.17	55.61	25.14	12.56	1:2.002: 4.428
$CuFe_2O_4$ NFs	5.92	55.8	25.25	13.03	1:1.938: 4.283
$MnFe_2O_4$ NFs	5.19	56.66	25.36	12.77	1:1.986: 4.437

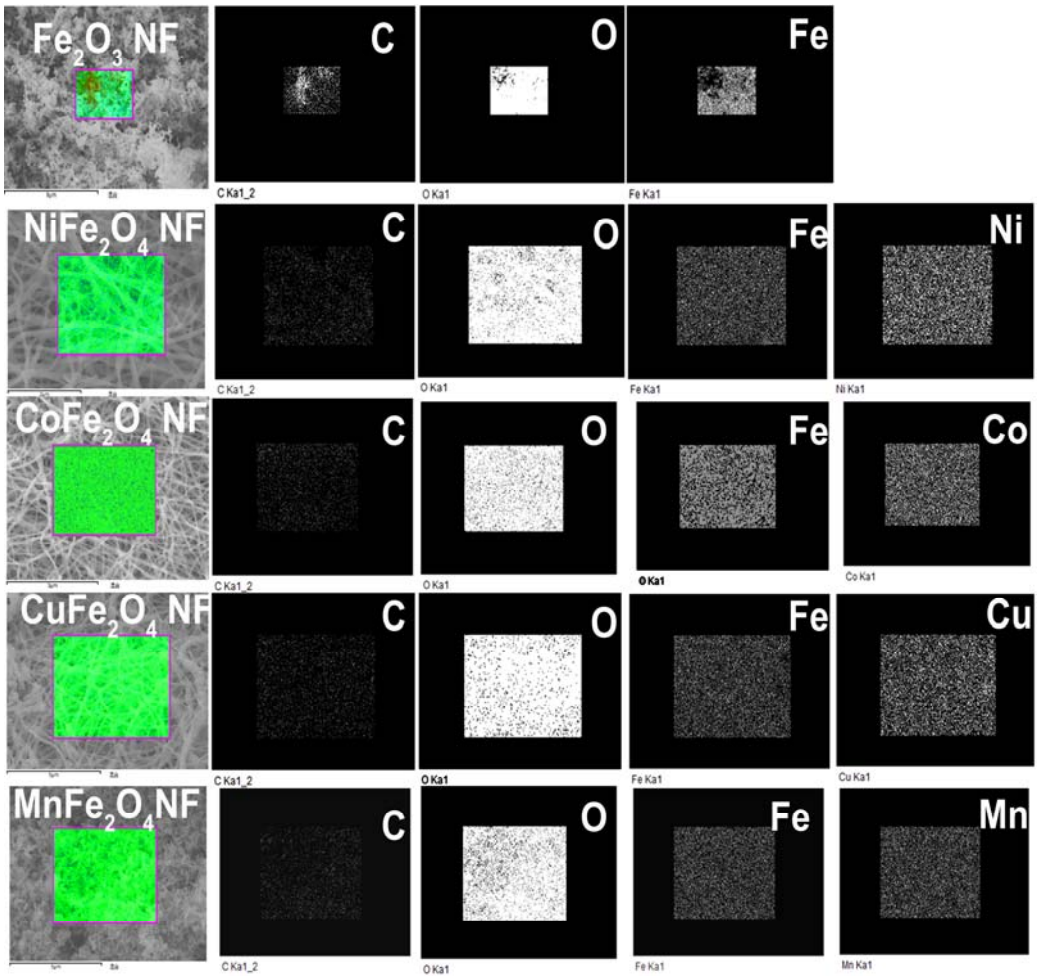

Fig. S2 Elemental mapping images acted on the 3D net-like Fe_2O_3, $CoFe_2O_4$, $NiFe_2O_4$, $CuFe_2O_4$, and $MnFe_2O_4$ NFs for the C, O, Fe, and M elements. Characterization results evidently reveal the extremely homogeneous co-existence and uniform distribution of Fe, M, and O species from inside to outside in the whole films, on the other hand, a small quantity of C species appear in all samples.

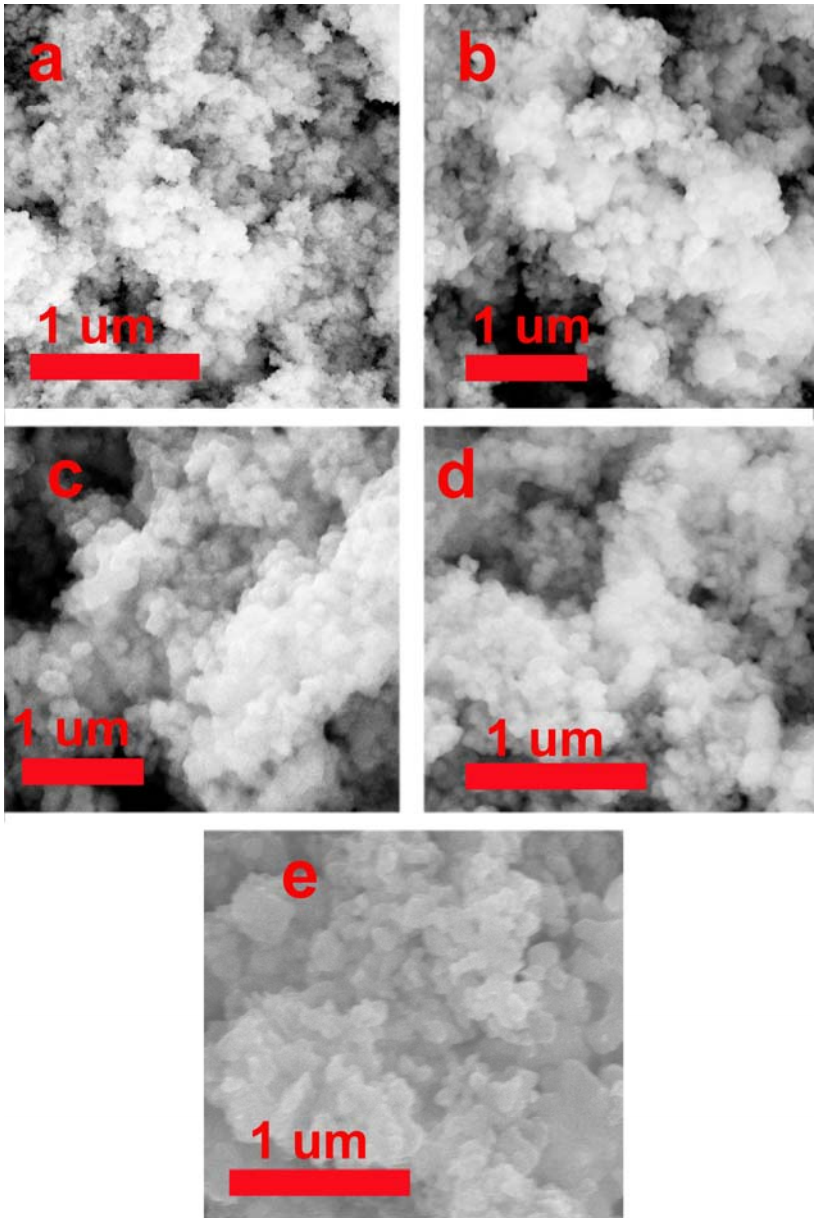

Fig. S3 Typical SEM images of the Fe_2O_3 (a), $CoFe_2O_4$ (b), $NiFe_2O_4$ (c), $CuFe_2O_4$ (d), and $MnFe_2O_4$ (e) NPs samples.

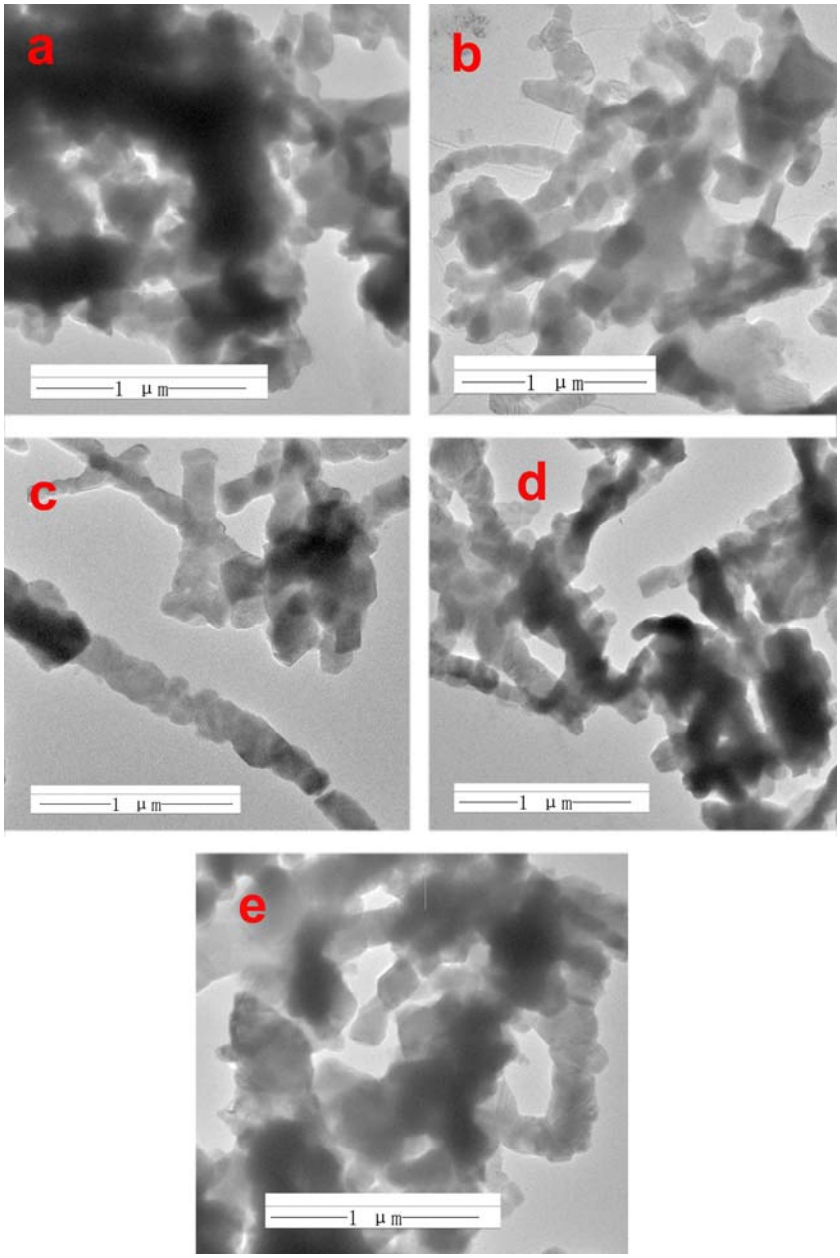

Fig. S4 Typical TEM images of the Fe_2O_3 (a), $CoFe_2O_4$ (b), $NiFe_2O_4$ (c), $CuFe_2O_4$ (d), and $MnFe_2O_4$ (e) NFs based nanofilms.

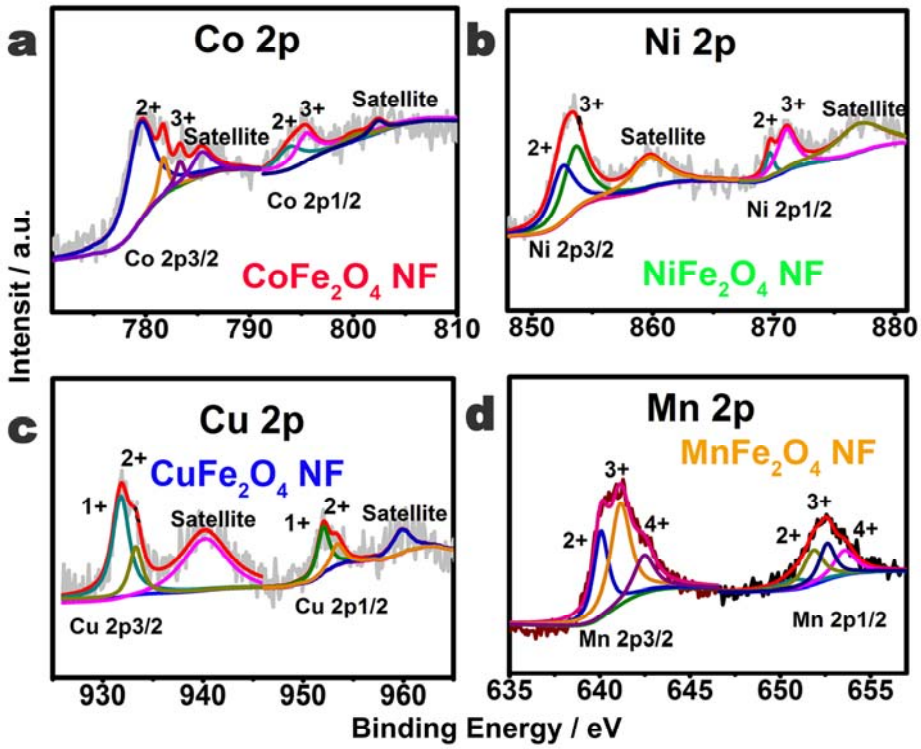

Fig. S5 M 2p for the $CoFe_2O_4$, $NiFe_2O_4$, $CuFe_2O_4$, and $MnFe_2O_4$ NFs.

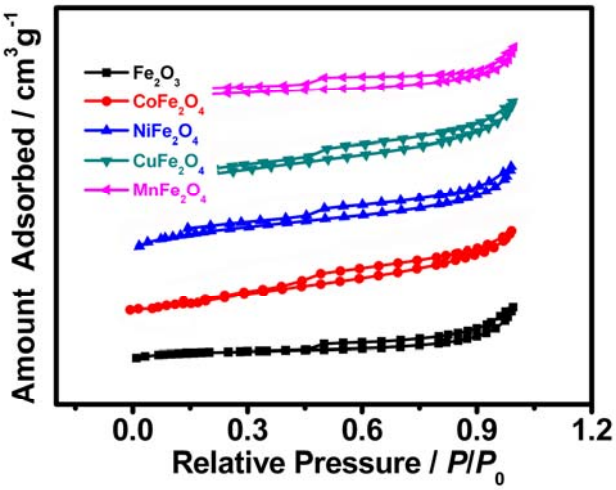

Fig. S6 Nitrogen adsorption-desorption isotherms of the Fe_2O_3, $CoFe_2O_4$, $NiFe_2O_4$, $CuFe_2O_4$ and $MnFe_2O_4$ NFs.

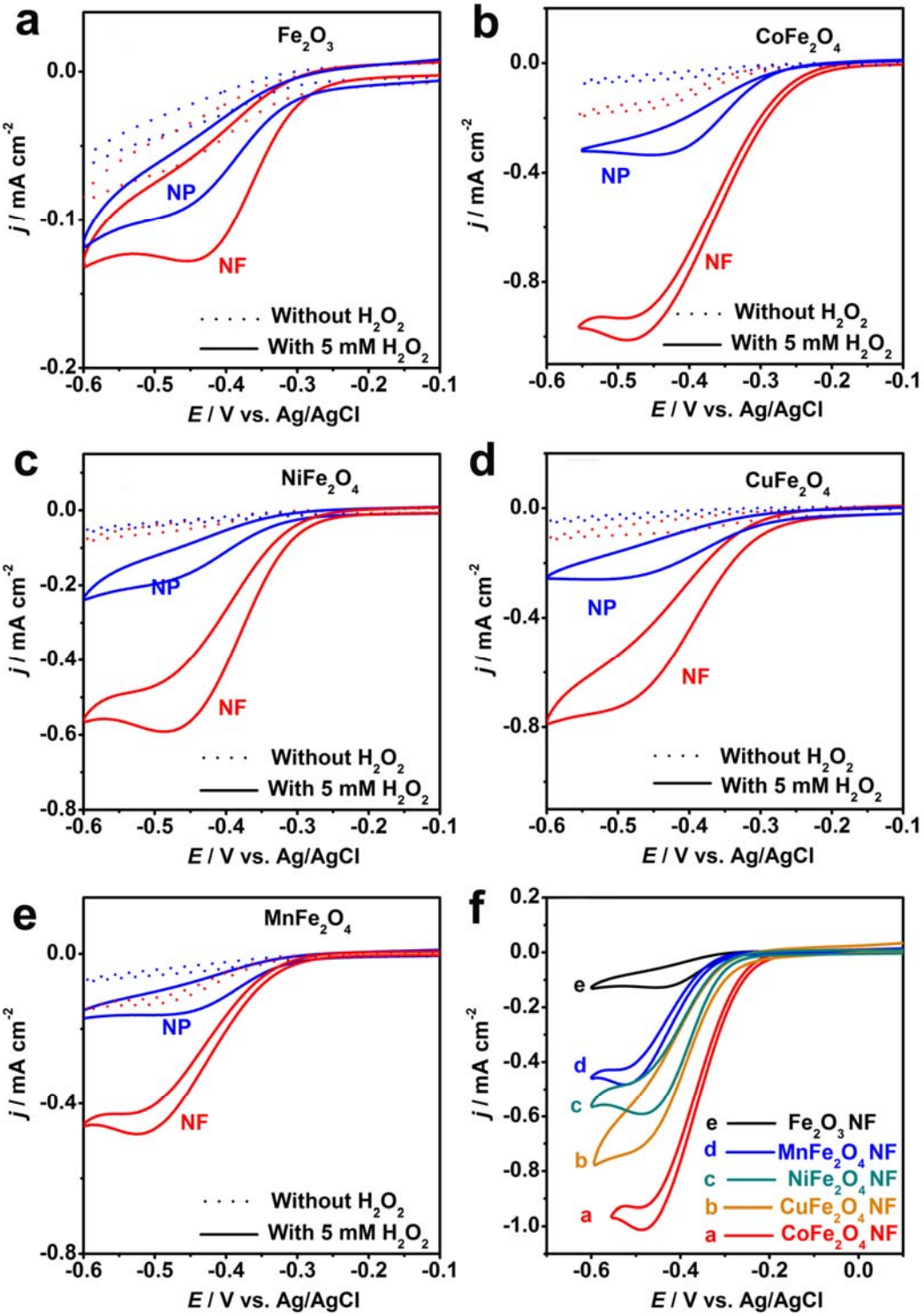

Fig. S7. Cyclic voltammograms of Fe_2O_3 NFs and Fe_2O_3 NPs (a), $CoFe_2O_4$ NFs and $CoFe_2O_4$ NPs (b), $NiFe_2O_4$ NFs and $NiFe_2O_4$ NPs (c), $CuFe_2O_4$ NFs and $CuFe_2O_4$ NPs (d), and $MnFe_2O_4$ NFs and $MnFe_2O_4$ NPs (e) in N_2 saturated 0.1 M KOH electrolyte with 5 mM H_2O_2 (solid lines) and without 5 mM H_2O_2 (dot lines) at a scan rate of 50 mV s^{-1}. (f) Cyclic voltammograms of $CoFe_2O_4$ NFs in comparison to those for Fe_2O_3, $NiFe_2O_4$, $CuFe_2O_4$, and $MnFe_2O_4$ NFs in N_2 saturated 0.1 M KOH electrolyte containing 5 mM H_2O_2 at a scan rate of 50 mV s^{-1}.

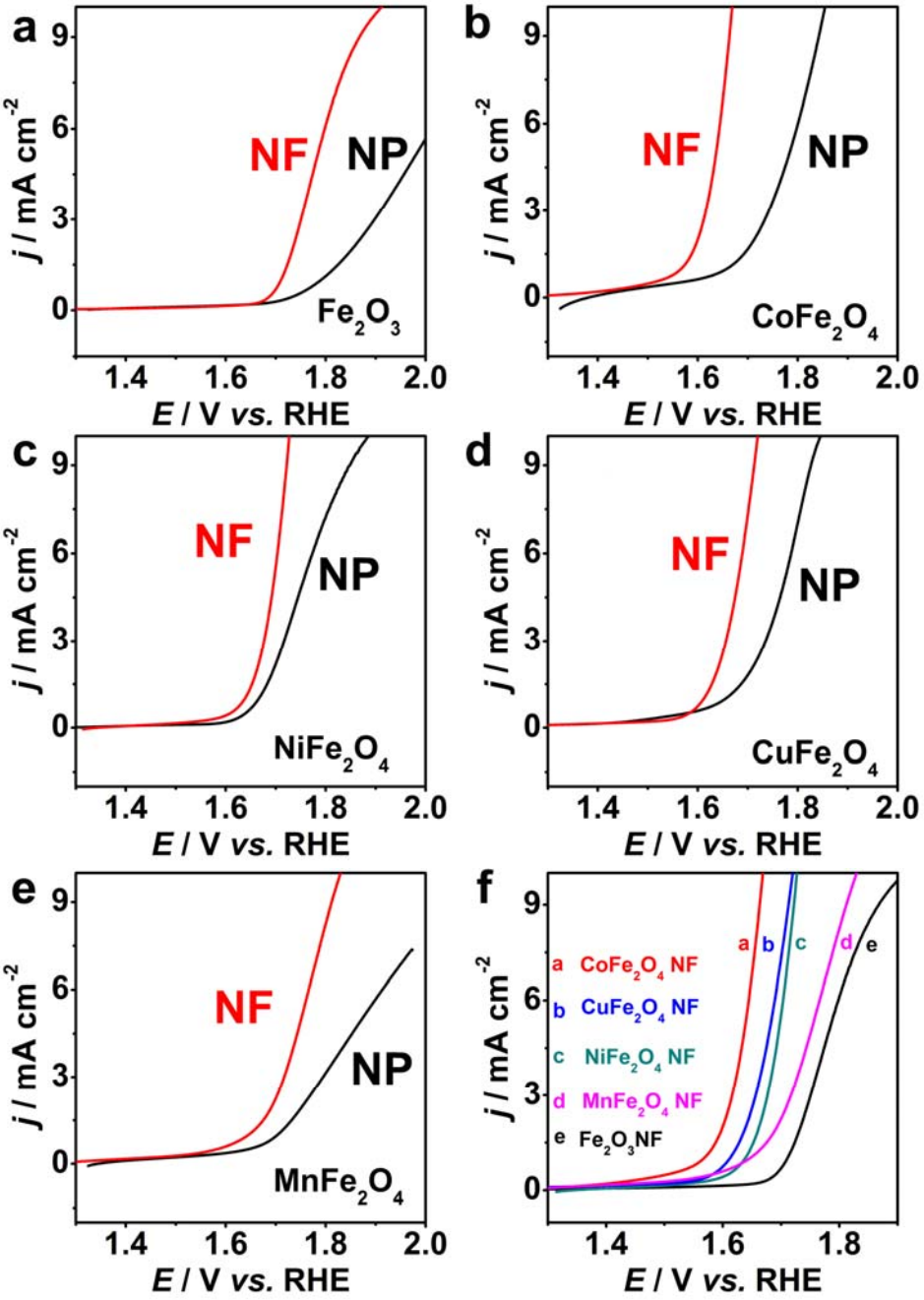

Fig. S8 The oxygen electrochemical catalysis on Fe_2O_3 NFs and Fe_2O_3 NPs (a), $CoFe_2O_4$ NFs and $CoFe_2O_4$ NPs (b), $NiFe_2O_4$ NFs and $NiFe_2O_4$ NPs (c), $CuFe_2O_4$ NFs and $CuFe_2O_4$ NPs (d), and $MnFe_2O_4$ NFs and $MnFe_2O_4$ NPs (e) in 0.1 M KOH electrolyte. (f) LSV plots of $CoFe_2O_4$ NFs in comparison to those for Fe_2O_3, $NiFe_2O_4$, $CuFe_2O_4$, and $MnFe_2O_4$ NFs.

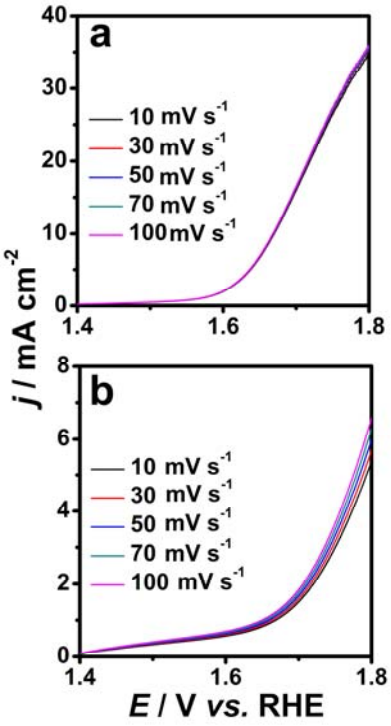

Fig. S9 LSV plots recorded on $CoFe_2O_4$ NFs (a) and $CoFe_2O_4$ NPs (b) at different scan rates from 10 to 100 mV s^{-1}. At the potential of 1.8 V vs. RHE, the $CoFe_2O_4$ NFs only displays a slight current increase of about 1.59 %, however, the $CoFe_2O_4$ NPs shows significant current increase of 22.48 % under the similar testing condition.

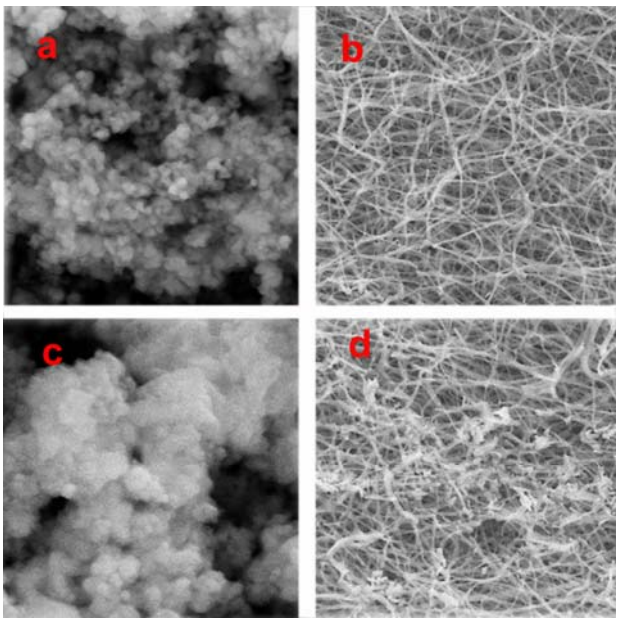

Fig. S10 SEM images of the $CoFe_2O_4$ NPs (a) and $CoFe_2O_4$ NFs (b) samples before the durability test. SEM images of the $CoFe_2O_4$ NPs (C) and $CoFe_2O_4$ NFs (d) samples after the durability test.

As shown in Fig. S10, to further understand the different durability behaviors of the $CoFe_2O_4$ NPs and $CoFe_2O_4$ NFs, morphological evolutions of the two catalysts were

also investigated by SEM. It is clear that before the durability test, the $CoFe_2O_4$ NPs are constructed by some large particles (Fig. S10a); the $CoFe_2O_4$ NFs display the special fiber morphology and hierarchical net-works and possess abundant micro/meso/macropores both on the surface and within the films (Fig. S10b). After the durability test, the $CoFe_2O_4$ NPs have aggregated into large cakes (Fig. S10c); however, no obvious aggregation is observed for the $CoFe_2O_4$ NFs (Fig. S10d). The special fiber morphology and hierarchical net-works with abundant micro/meso/macropores of the $CoFe_2O_4$ NFs indeed has very strong structural stability, which will invariably afford enough solid-liquid-gas regions required for the transport of reactants and products during the process of OER. Thus, the $CoFe_2O_4$ NFs show the $CoFe_2O_4$ NFs shows insignificant performance attenuation (< 8 %) after operation for 20000 s. On the contrary, as the particles of the $CoFe_2O_4$ NPs aggregate into large cakes gradually, the surface of $CoFe_2O_4$ NPs cannot afford enough solid-liquid-gas regions required for the transport of reactants and products during the process of OER. Thus, the current density will rapidly decrease for the $CoFe_2O_4$ NPs during the chronoamperometric analysis (after operation for 20000 s, a rapid activity decrease (> 30 %) will be found).The strong durability and enhanced performance indicate that the 3D net-like spinel-type $CoFe_2O_4$ NF film is an efficient OER catalyst.

Table S2

Comparison of the performances between the proposed $CoFe_2O_4$ NFs and those H_2O_2 biosensors containing cobalt, nickel, iron, copper, and/or manganese.

Working electrode	Linear range (mM)	Sensitivity ($\mu A\ mM^{-1}\ cm^{-2}$)	Detection limit (μM)	Applied potential (V)	Response time (s)	Reference
$CoFe_2O_4$ NF	0.005-3 3-17	45.25 25.94	0.5	-0.46 vs. Ag/AgCl	<3	This work
$Co_xNi_{1-x}Fe_2O_4$	1.0×10^{-5}-1.0	-	3.0×10^{-3}	+ 0.5 vs. Ag/AgCl	-	[1]
MnO_2/OMC	5×10^{-4}-0.6	806.8	0.07	+ 0.45 vs. Ag/AgCl	7	[2]
Fe_3O_4 thin-film	up to 0.7	432.2	1	−0.4 vs. Ag/AgCl	-	[3]
$LaNiO_3$ NFs	5×10^{-5}-1	1135.88	0.034	+ 0.6 vs. Ag/AgCl	-	[4]
Cobalt manganese oxides	0.1-25	2.9	15	-0.65 vs. Ag/AgCl	<10	[5]
$NiFe_2O_4$ NPs	0.01- 2	0.2596	2	−0.1 V vs. SCE	<5	[6]
Cu_2O/GNs	0.3-7.8	-	20.8	-0.4 vs. Ag/AgCl	<7	[7]
Hollow CuO	5×10^{-4}-1	1746.50	0.022	+0.6 vs. Ag/AgCl	2	[8]
Fe_3O_4-RGO	0.1-6	-	3.2	-0.3 vs. SCE	5	[9]
NiHCF/CS/CNTs	0.04–5.6	654	0.28	-2 vs. SCE	2	[10]
MnO_2-Ag	2.4×10^{-4}-4	-	0.24	-0.5 vs. Ag/AgCl	3	[11]
Cu_2O–rGO	0.03–12.8	19.5	21.7	-0.4 vs. SCE	2	[12]
Au –MnO_2–rGO	0.022–12.6	980	0.05	-2 vs. SCE	5	[13]
PPDA@Fe_3O_4	5×10^{-4}- 0.4	-	0.21	-0.4 vs.SCE	4	[14]
Cu–Co alloy	1×10^{-4}-11	-	0.75	-0.4 vs. Ag/AgCl	-	[15]

References

1. L. Luo, Y. Zhang, F. Li, X. Si, Y. Ding, D. Deng and T. Wang, *Analytica Chimica Acta*, 2013, **788**, 46-51.
2. L. Luo, F. Li, L. Zhu, Z. Zhang, Y. Ding and D. Deng, *Electrochimica Acta*, 2012, **77**, 179-183.
3. J. Yang, H. Xiang, L. Shuai and S. Gunasekaran, *Analytica Chimica Acta*, 2011, **708**, 44-51.

4. B. Wang, S. Gu, Y. Ding, Y. Chu, Z. Zhang, X. Ba, Q. Zhang and X. Li, *Analyst*, 2013, **138**, 362-367.

5. C.-C. Kuo, W.-J. Lan and C.-H. Chen, *Nanoscale*, 2014, **6**, 334-341.

6. L. Luo, L. Zhu, Y. Xu, L. Shen, X. Wang, Y. Ding, Q. Li and D. Deng, *Microchimica Acta*, 2011, **174**, 55-61.

7. M. Liu, R. Liu and W. Chen, *Biosensors & Bioelectronics*, 2013, **45**, 206-212.

8. B. Wang, L. Luo, Y. Ding, D. Zhao and Q. Zhang, *Colloids and Surfaces B-Biointerfaces*, 2012, **97**, 51-56.

9. Y. Ye, T. Kong, X. Yu, Y. Wu, K. Zhang and X. Wang, *Talanta*, 2012, **89**, 417-421.

10. Z. Wang, X. Hao, Z. Zhang, S. Liu, Z. Liang and G. Guan, *Sensors and Actuators B-Chemical*, 2012, **162**, 353-360.

11. Q. Han, P. Ni, Z. Liu, X. Dong, Y. Wang, Z. Li and Z. Liu, *Electrochemistry Communications*, 2014, **38**, 110-113.

12. F. Xu, M. Deng, G. Li, S. Chen and L. Wang, *Electrochimica Acta*, 2013, **88**, 59-65.

13. L. Wang, M. Deng, G. Ding, S. Chen and F. Xu, *Electrochimica Acta*, 2013, **114**, 416-423.

14. M. Baghayeri, E. N. Zare and M. M. Lakouraj, *Biosensors & Bioelectronics*, 2014, **55**, 259-265.

15. H.-B. Noh, K.-S. Lee, P. Chandra, M.-S. Won and Y.-B. Shim, *Electrochimica Acta*, 2012, **61**, 36-43.